



Mechanism and function of root circumnutation

Isaiah Taylor^{a,b,1} , Kevin Lehner^{a,1,2}, Erin McCaskey^{c,3} , Niba Nirmal^{a,3}, Yasemin Ozkan-Aydin^c , Mason Murray-Cooper^c, Rashmi Jain^d , Elliot W. Hawkes^e , Pamela C. Ronald^d , Daniel I. Goldman^c , and Philip N. Benfey^{a,b,4}

^aDepartment of Biology, Duke University, Durham, NC 27708; ^bHoward Hughes Medical Institute, Duke University, Durham, NC 27708; ^cSchool of Physics, Georgia Institute of Technology, Atlanta, GA 30332; ^dDepartment of Plant Pathology and the Genome Center, University of California, Davis, CA 95616; and ^eDepartment of Mechanical Engineering, University of California, Santa Barbara, CA 93106

Edited by R. Scott Poethig, University of Pennsylvania, Philadelphia, PA, and approved January 13, 2021 (received for review September 8, 2020)

Early root growth is critical for plant establishment and survival. We have identified a molecular pathway required for helical root tip movement known as circumnutation. Here, we report a multi-scale investigation of the regulation and function of this phenomenon. We identify key cell signaling events comprising interaction of the ethylene, cytokinin, and auxin hormone signaling pathways. We identify the gene *Oryza sativa* histidine kinase-1 (*HK1*) as well as the auxin influx carrier gene *OsAUX1* as essential regulators of this process in rice. Robophysical modeling and growth challenge experiments indicate circumnutation is critical for seedling establishment in rocky soil, consistent with the long-standing hypothesis that root circumnutation facilitates growth past obstacles. Thus, the integration of robotics, physics, and biology has elucidated the functional importance of root circumnutation and uncovered the molecular mechanisms underlying its regulation.

circumnutation | rice roots | histidine kinase-1

During the life cycle of a plant, penetration of roots into soil is a fundamental yet physically challenging task (1, 2). This is especially true for the primary root (the first root to emerge from the seed) because it provides the seedling with its sole source of anchorage and water/nutrient absorption and because it must enter the soil without other mechanical support (3, 4). The emergent primary root faces two related challenges: It must grow into a heterogeneous soil substrate wherever the seed lands, and it must do so when the seed is otherwise unanchored. Species adapted to growing in wetlands, such as rice, face the added complication of establishing during sporadic floods that pose a catastrophic danger of washout (5–7). Thus, the earliest stages of root growth represent a critical window of survival when rapid and robust root penetration into soil is essential. It is, therefore, logical to posit that primary root growth strategies have evolved to meet the challenges arising from the myriad growth conditions seedling roots encounter.

One root behavior with a long-hypothesized role in promoting root penetration of soil is the helical movement of the root tip known as circumnutation. Charles and Francis Darwin first observed evidence of root circumnutation during their study of plant tropisms and suggested it may be a strategy to allow roots to grow past obstacles (8). Since this time, circumnutation of the rice primary root has gradually been adopted as an important model for this process (e.g., refs. 9 and 10). For instance, a study of seven rice varieties established that the angle of the root tip during circumnutation was positively correlated with seedling establishment in flooded field conditions (9). However, progress has been hindered by the lack of genetic mutants specifically defective in root circumnutation, which would allow direct functional characterization of circumnutation in an isogenic background. In this work, we report the identification of such a mutant in the *Oryza sativa* histidine kinase-1 (*HK1*) gene. We show that *HK1* is a key regulator of cross-talk between multiple hormone signaling pathways, and we employ *in planta* and robophysical experimentation to provide strong support for the hypothesis that circumnutation is an adaptation facilitating root growth around obstacles.

Results

Mutants in the *HK1* Gene Fail to Undergo Root Circumnutation. To identify regulators of early root growth strategies in rice, we performed a genetic screen on a subset of a sequenced mutant population in the model rice cultivar KitaakeX (11–13). Plants were grown in transparent gel media, and the developing root systems were imaged over the course of several days using a previously described phenotyping system (14, 15). From this screen, we isolated three allelic mutants each exhibiting a ~50% increase in primary root length, all harboring lesions in the *HK1* gene (Fig. 1A and *SI Appendix*, Fig. S1). To understand the dynamics of root elongation in the mutants, we used a modified version of our phenotyping platform employing automated time-lapse imaging to monitor growth every 15 min for several days following germination. Imaging revealed wild-type roots undergoing striking helical movement of the tip known as circumnutation, with the mutants appearing to grow predominantly downward (*Movie S1*). To visualize this phenomenon, we tracked the position of the root tip in wild type and mutants for 2 d after germination. We then estimated a central axis of root growth using locally estimated scatterplot smoothing (loess) regression and plotted the two-dimensional (2D) projection of displacement from this central axis at each 15-min time point (Fig. 1B and *SI Appendix*, Fig. S1). From this analysis, we observed that in wild type, circumnutation typically becomes regular within a day after germination and approaches a maximum in both amplitude and period by ~48 h. In contrast, the mutant

Significance

Root growth in soil is complex. With limited sensory input, roots must navigate an environment containing heterogeneities such as rocks and compaction. The ability of roots to penetrate soil is crucial for water and nutrient uptake as well as mechanical anchorage. Here, we describe a molecular framework controlling helical root growth known as circumnutation. Functional characterization of circumnutation is consistent with the hypothesis that it is crucial for exploratory behavior and substrate penetration. This work lays a foundation for an integrated understanding of how roots grow in soil.

Author contributions: I.T., K.L., E.M., Y.O.-A., R.J., E.W.H., P.C.R., D.I.G., and P.N.B. designed research; I.T., K.L., E.M., N.N., Y.O.-A., M.M.-C., and R.J. performed research; I.T., K.L., E.M., Y.O.-A., M.M.-C., R.J., E.W.H., P.C.R., D.I.G., and P.N.B. contributed new reagents/analytic tools; I.T., K.L., E.M., and R.J. analyzed data; and I.T. and K.L. wrote the paper.

The authors declare no competing interest.

This article is a PNAS Direct Submission.

Published under the [PNAS license](#).

¹I.T. and K.L. contributed equally to this work.

²Present address: Department of Agricultural Biology, Colorado State University, Fort Collins, CO 80521.

³E.M. and N.N. contributed equally to this work.

⁴To whom correspondence may be addressed. Email: philip.benfey@duke.edu.

This article contains supporting information online at <https://www.pnas.org/lookup/suppl/doi:10.1073/pnas.2018940118/-DCSupplemental>.

Published February 19, 2021.

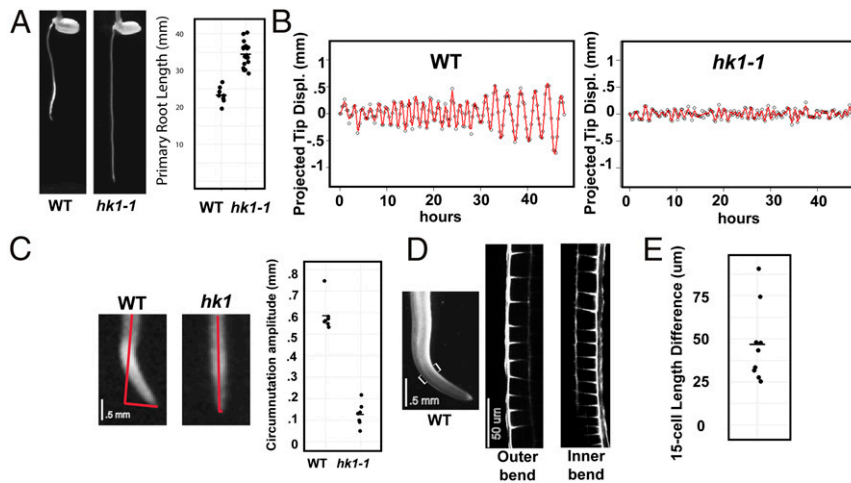


Fig. 1. Phenotypic analysis of the *hk1* mutant. (A) Primary root depth 2 d after germination for wild type and the *hk1-1* mutant. $n = 8$ and 18 primary roots for wild type and mutant, respectively. Two-sided Wilcoxon Rank Sum test P value = 7.1×10^{-5} . The horizontal dash indicates mean value. (B) Two-dimensional projected displacement of root tip from central axis of growth every 15 min for 48 h after germination. Red plots represent natural cubic splines fit to the data for visualization. (C) Quantification of average radius of circumnutation in wild type and *hk1* between 40 and 48 h after germination. $n = 7$ primary roots for each genotype. Two-sided Wilcoxon Rank Sum test P value = 0.0005828. The horizontal dash indicates mean value. (D) Example circumnutating wild-type primary root exhibiting higher epidermal cell elongation on the outer bend compared to the inner bend. (E) Quantification of the difference between outer and inner length of the region of 15 epidermal cells flanking the maximal bend in wild type, with $n = 9$. Two-sided Wilcoxon Signed Rank test P values = 0.003906. The horizontal dash indicates mean value.

never enters into an organized circumnutational pattern, and the root tip remains situated close to the central axis of growth.

In wild-type roots, circumnutation is driven by a pronounced bending of the root, typically occurring 1 to 2 mm from the tip, in the region of rapid cellular elongation (16). To quantify this phenotype, we calculated the amplitude of tip displacement for several wild-type roots over the course of 8 h after circumnutation had been strongly initiated (Fig. 1C and *Materials and Methods*). Wild type had a mean amplitude of tip displacement of 0.60 mm (± 0.07 mm SD), which corresponds to the radius of the cylinder circumscribed by the root tip as it revolves around its central axis (Fig. 1C). In contrast, the mutant exhibits erratic, small amplitude displacement with a mean of ~ 0.13 mm (± 0.05 mm SD) over the same timeframe (Wilcoxon Rank Sum test P value = 0.00058, Fig. 1C).

Circumnutation Is Associated with Higher Rates of Cell Elongation on the Outer Bend of the Root. Root bending during circumnutation is reminiscent of root bending during response to gravitational stimulus, a process driven by differential cell elongation on the upper and lower sides of the turning root (reviewed in ref. 17). Examination of epidermal cells on the outer and inner bend of circumnutating wild-type roots consistently revealed a lower rate of elongation on the inner bend (Fig. 1D), suggesting root bending occurring during circumnutation is geometrically analogous to that occurring during graviresponse. To quantify this effect, we recorded the epidermal cell length on the inner and outer side of nine circumnutating wild-type roots in a region of 15 cells flanking a line bisecting the root at the region of maximal bending (*SI Appendix, Fig. S2*). We calculated the difference between the length of this region of cells on the outer and inner side of the root and found a consistent decrease in the length spanned by 15 cells on the inner side of the bend (Wilcoxon Signed Rank test P value = 0.003906, Fig. 1E). This result suggests circumnutation is driven by transient, circumferentially localized differential elongation between the inner and outer sides of the bending root. It is interesting to note that while many periodic plant growth processes (such as root waving in *Arabidopsis*) exhibit fixed chirality (18, 19), we found that rice roots appear to circumnutate in equal proportions in either clockwise or counterclockwise orientation (*SI Appendix, Fig. S3*). This implies a

fundamental difference in the mechanism of root waving in *Ara-**bidopsis* and circumnutation in rice.

Evidence That Ethylene Positively Regulates Circumnutation. The occurrence of root circumnutation in rice has been described in a number of studies (9, 10, 20). However, the mechanistic regulation of this process is still largely undefined. *HK1* has recently been shown to positively regulate ethylene signaling in rice roots downstream of ethylene receptors (21). This signaling pathway was shown to restrict root elongation, but a connection between ethylene signaling and circumnutation has not been established. To determine if ethylene signaling regulates circumnutation, we applied the ethylene receptor inhibitor 1-methylcyclopropene (1-MCP) to circumnutating wild-type roots. This treatment led to a rapid and dramatic cessation of circumnutation and a sudden increase in the rate of root elongation (*SI Appendix, Fig. S4* and *Movie S2*). This result is consistent with a model in which ethylene activates *HK1* to promote circumnutation, leading to a reduction in the rate of root elongation.

***HK1* Activates Downstream Cytokinin-Type Signaling to Regulate Circumnutation.** We next focused on understanding the mechanism of downstream regulation of circumnutation. *HK1* encodes an active histidine kinase with homology to cytokinin receptors but lacks a predicted cytokinin binding domain (21, 22) (*SI Appendix, Fig. S5*). Ethylene has recently been shown to mediate activation of the *HK1* protein leading to direct phosphorylation of histidine-containing phosphotransfer/AHP proteins, well-characterized effectors that function downstream of receptors in canonical cytokinin signaling (21). This *HK1*-mediated AHP phosphorylation in turn feeds into cytokinin responsive transcriptional regulation (21). These results indicate regulation of *HK1* represents a previously unobserved point of cross-talk between ethylene and cytokinin signaling.

We reasoned if the *HK1* pathway activates downstream cytokinin signaling, and reduction of this signaling causes the *hk1* mutant phenotype, we could rescue circumnutation by treating the mutant with exogenous cytokinin. Consistent with this hypothesis, treatment with the naturally occurring cytokinin, *trans*-zeatin, led to a rescue of circumnutation, albeit with a slight delay in onset,

and an increase in the mean amplitude of tip displacement from 0.11 mm (± 0.03 mm SD) in control roots to 0.64 mm (± 0.11 mm SD) in *trans*-zeatin-treated roots (Wilcoxon Rank Sum test P value = 0.01587, Fig. 2A and Movie S3). RNA-Sequencing (Seq) analysis of the distal 2 mm of root tip revealed that transcript abundance levels of canonical cytokinin signaling-induced type A response regulator genes are reduced between 45 to 90% in the *hk1* mutant (Fig. 2B and SI Appendix, Dataset S1). Similar RNA-Seq analysis demonstrated that this reduction is reversed upon treatment with *trans*-zeatin (Fig. 2B). Furthermore, we found a strong positive relationship between global gene expression changes comparing log (fold change) of wild type/mutant with log (fold change) of mutant \pm *trans*-zeatin (SI Appendix, Fig. S6). These results indicate *HK1* activates downstream cytokinin signaling to regulate circumnutation. An initial diagram of our findings is displayed in Fig. 2C. An open question for future study is whether canonical cytokinin receptor signaling also makes a meaningful contribution to the regulation of circumnutation, or if the *trans*-zeatin-induced rescue of *hk1* represents artificial stimulation of downstream signaling by exogenous cytokinin.

Evidence That *HK1* Regulates Circumnutation by Controlling Auxin Transport and Response. We next sought a mechanism to link this signaling pathway to regulation of cell elongation during circumnutation. Root bending during the graviresponse is driven by directional transport of the plant hormone auxin to the outer cell layers of the lower side of the root by the coordinated action of auxin influx and efflux carriers (reviewed in refs. 17, 23, and 24). Accumulation of auxin on the lower side of the root then inhibits cell elongation, causing downward tip reorientation. Application of auxin transport inhibitors to the roots of pea seedlings has been shown to block circumnutation (25), suggesting a connection between auxin transport and root bending during circumnutation. Additionally, regulation of auxin transport and signaling have been implicated in a variety of oscillatory root growth phenomena in *Arabidopsis* (18, 26–32), although interpretation of the underlying physical basis for these growth responses has been challenging (19, 30, 33).

To investigate the involvement of auxin in regulating circumnutation, we first examined our RNA-Seq data and discovered that in the *hk1* mutant, there is a reduction in a large number of canonical auxin response genes, such as those encoding AUX/indole-3-acetic acid (IAA) proteins (Fig. 3A) and small auxin up-regulated RNA (SAUR) genes (SI Appendix, Fig. S7). We also noted a general restoration of expression for these genes in the mutant treated with *trans*-zeatin (Fig. 3A and SI Appendix, Fig. S7), consistent with the hypothesis that an auxin response is involved in regulating circumnutation. To test this hypothesis, we grew wild-type roots in media containing the auxin efflux inhibitor *N*-1-naphthylphthalamic acid (NPA). This treatment resulted in near-complete inhibition of circumnutation, as evidenced by a reduction in the mean amplitude of tip displacement from 0.62 mm (± 0.10 mm SD) in control roots to 0.11 mm (± 0.12 mm SD) in NPA-treated roots (Wilcoxon Rank Sum test P value = 0.004329, Fig. 3B and Movie S4), indicating auxin transport plays a key role during this process. Next, we reasoned if the phenotype of *hk1* is due to defects in auxin transport, we may be able to rescue circumnutation in the mutant by the addition of exogenous auxin. Because auxin has a potent inhibitory effect on root elongation, we allowed plants to grow untreated for up to 1 d in hydroponic conditions before supplementing the media with auxin. We found that the predominant naturally occurring auxin, IAA, did not rescue the circumnutation defect of *hk1* at any concentration tested (Movie S5). In contrast, the membrane-permeable synthetic auxin 1-naphthaleneacetic acid (1-NAA), but not the structurally related nonauxinic analog 2-NAA, rescued the defect of the *hk1* mutant, with an increase in mean tip displacement from 0.19 mm (± 0.07 mm SD) in control roots to 0.59 mm (± 0.14 mm SD) in roots treated with 1-NAA (Wilcoxon Rank Sum test P value = 0.0005828, Fig. 3C and Movie S5). It is notable that the period of circumnutation is substantially higher in 1-NAA-treated *hk1* compared to wild-type or *trans*-zeatin-treated *hk1* (Figs. 1B, 2A, and 3C). This may be due to general reduction in root cell elongation upon treatment with exogenous auxin or perhaps represents differing rates of auxin transport between synthetic 1-NAA and endogenous IAA.

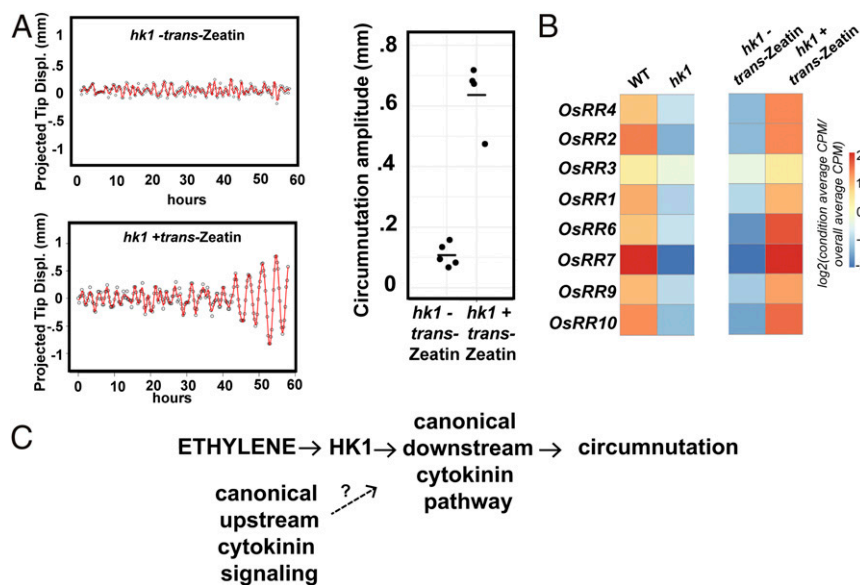


Fig. 2. Characterization of molecular signaling downstream of *HK1*. (A) Example root tip traces and quantification of average radius of circumnutation in *hk1* treated with *trans*-zeatin between 50 and 58 h after germination. $n = 5$ and 4 primary roots for untreated and treated, respectively. Two-sided Wilcoxon Rank Sum test P value = 0.01587. The horizontal dash indicates mean value. For the treated samples, *trans*-zeatin was included in the media for the entire duration of the experiment. (B) Relative expression level of eight root tip expressed cytokinin signaling regulated Type-A Response Regulator genes in wild type versus *hk1* and *hk1* \pm cytokinin. (C) Diagram of proposed signaling pathway regulating of circumnutation. The uncertain contribution of canonical upstream cytokinin signaling to circumnutation is indicated by a question mark.

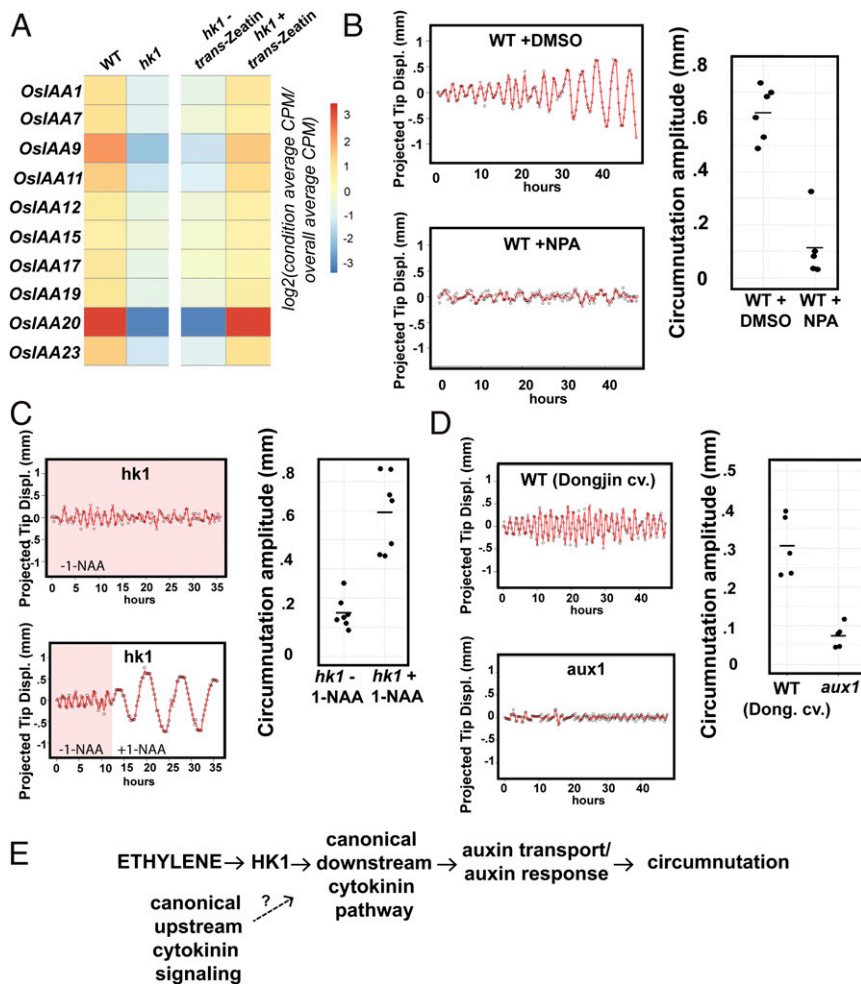


Fig. 3. Evidence auxin transport and response regulate circumnutation. (A) Relative expression level of 10 root tip expressed *AUX/IAA* genes in wild type versus *hk1* and *hk1*^{-/-} cytokinin. (B) Example root tip traces and quantification of average radius of circumnutation in wild-type plants treated with NPA. *n* = 6 and 5 primary roots for untreated and treated, respectively. Two-sided Wilcoxon Rank Sum test *P* value = 0.004329. The horizontal dash indicates mean value. NPA/DMSO was included in the growth media for the entire duration of the experiment. (C) Example root tip traces and quantification of average radius of circumnutation in *hk1* plants grown hydroponically after addition of 200 nM 1-NAA. *n* = 7 primary roots for both untreated and treated. Two-sided Wilcoxon Rank Sum test *P* value = 0.0005828. The horizontal dash indicates mean value. 1-NAA was added to hydroponic media ~12 to 24 h after germination. (D) Example root tip traces and quantification of average radius of circumnutation in wild type (Dongjin cultivar) and *aux1*. *n* = 5 primary roots for each genotype. Two-sided Wilcoxon Rank Sum test *P* value = 0.007937. The horizontal dash indicates mean value. (E) Diagram of proposed signaling pathway regulating of circumnutation. The uncertain contribution of canonical upstream cytokinin signaling to the regulation of circumnutation is indicated by a question mark.

Mutation of the Auxin Importer Gene *OsAUX1* Blocks Circumnutation.

The specific ability of 1-NAA to rescue circumnutation suggests a model of regulation by *HK1*. 1-NAA is able to efficiently cross the plasma membrane from the apoplast, independent of the well-studied auxin importer *AUX1* (34, 35). After entry into the cytosol, 1-NAA is then an efficient substrate for the auxin efflux machinery (34). Thus, the ability of 1-NAA to rescue the *hk1* phenotype suggests auxin import, but not export, is critically impaired in the *hk1* mutant. To investigate this possibility, we reexamined our RNA-Seq data and noted transcript levels of the auxin importer gene *OsAUX1* are reduced ~30% in the *hk1* mutant, and its abundance is restored to approximately wild-type levels in the mutant treated with cytokinin (*SI Appendix*, Fig. S8). To test if *AUX1* is a regulator of circumnutation, we analyzed an *aux1* mutant isolated in the Dongjin cultivar of rice and found, in addition to its previously described agravitropic and enhanced primary root length phenotypes (36, 37), it exhibited a complete loss of circumnutation as evidenced by a reduction in the mean amplitude of tip displacement from 0.30 mm (± 0.08 mm SD)

in wild type to 0.07 mm (± 0.03 mm SD) in *aux1* (Wilcoxon Rank Sum test *P* value = 0.007937, Fig. 3D and *Movie S6*). Interestingly, the ability of 1-NAA to rescue circumnutation in *hk1* is reminiscent of the ability of 1-NAA to rescue gravitropic response in the *Arabidopsis aux1* mutant (38), consistent with a model in which defects in circumnutation in *hk1* are due to defects in auxin import. Collectively, our results indicate *HK1* regulates an auxin response controlling circumnutation, at least in part, by controlling *AUX1*-mediated auxin influx capacity. Importantly, our results imply that the *hk1* mutant still possesses the auxin efflux capacity capable of producing circumnutation. An updated diagram based on these findings is presented in Fig. 3E.

The *hk1* Mutant Is Defective in Exploration of Solid Surfaces. A previous study of root circumnutation across seven rice cultivars established a positive correlation between root tip angle during circumnutation in laboratory experiments and the success of seedling establishment in field conditions (9), supporting the hypothesis that circumnutation

promotes primary root colonization of soil. To further test this hypothesis, we performed functional studies on wild type and the *hkl1* mutant in artificial and natural growth substrates. The first experiment was motivated by a phenotype we observed when mutant roots reach the bottom of a growth container, where they often form restricted coils, in contrast to wild type, which grows along the surface distal to the site of contact (Fig. 4A). We hypothesized that this coiling behavior of *hkl1* mutants would reduce its ability to effectively explore hardened interfaces. To model this phenomenon, we used plastic surfaces with 2.5-mm diameter holes equally spaced at different densities in a square lattice. The surfaces were placed on hollow platforms of equal height in containers with gel-based media and imaged with a high-throughput automated system (Fig. 4B). At the highest hole density (5-mm spacing), both wild-type and *hkl1* primary roots were effective in encountering holes and continuing deeper growth (Fig. 4C). However, as hole density decreased, *hkl1* roots showed a pronounced reduction in success in encountering a hole (Fig. 4C and [Movie S7](#)). To quantify this effect, we employed logistic regression to model the probability of success in finding a hole as a function of spacing and genotype ([SI Appendix, Fig. S10](#)). We observed an effect of genotype translating to an overall estimated 12-fold increase in the odds of success in the wild type compared to mutant (estimated odds ratio, 95% Wald CI [3.43, 45.09]). These data indicate that wild-type roots are more effective in exploration and less affected by sparse hole density than *hkl1* mutants, providing a plausible mechanism to buffer against environmental uncertainty inherent in exploration of soil interfaces.

Robotic Simulation Demonstrates the Utility of Circumnutation in Obstacle Avoidance. To study mechanical principles underlying the function of circumnutation, we challenged a pneumatically actuated soft robophysical root model (described in refs. 39 and 40) with or without nutation in a variety of 2D obstacle courses ([Movie S8](#)). This device employs tip-based extension and is capable of generating

oscillatory 2D nutations isolated to the distal terminus when side actuators are sequentially inflated (Fig. 5A and B). Two differences between this model and biological root growth are that the robot grows and oscillates in only two dimensions, instead of three, and that the robotic root shortens the inner surface of a curve to pull the tip laterally, while the biological root lengthens the outer surface to push the tip. Despite these differences, the model is useful in that it enables dissection of the functional consequences of addition of a lateral growth component during root exploration in an experimentally tractable robotic system (41). Prior experiments demonstrated that nutating robotic roots are able to efficiently extend into a lattice of regularly spaced pegs, while nonnutating control robotic roots nearly always become stuck in the first two rows of the lattice (40).

To gain insight into the mechanism by which nutation improves penetration, we utilized video analysis of this experimental system to study what occurred when the robotic root encountered an obstacle. We hypothesized that nutating robotic roots would be able to contact obstacles nearly head-on yet pass, while nonnutating roots could only pass if they graze an obstacle. A plausible explanation is that nutation adds a lateral component to the force vector that the tip applies to the obstacle, making it more tangential; without nutation, this tip force is aligned with the axis of the root (Fig. 5D). Slipping along an obstacle to pass it only occurs when the tip force is sufficiently tangential to overcome the force of friction; thus, a nonnutating root with an axis-aligned tip force must contact an obstacle more tangentially than a nutating root (Fig. 5D). To test this hypothesis, we measured the contact angle of the tip (α , see inset of Fig. 5E and [SI Appendix, Fig. S8](#)) and compared the distribution of the contact angles where the robotic root successfully passed with and without nutation. In the nutating case, at even the lowest contact angles (most head-on contact), the success rate was over 80%. However, when the contact angle of a nonnutating root was less than 15° , the root tip

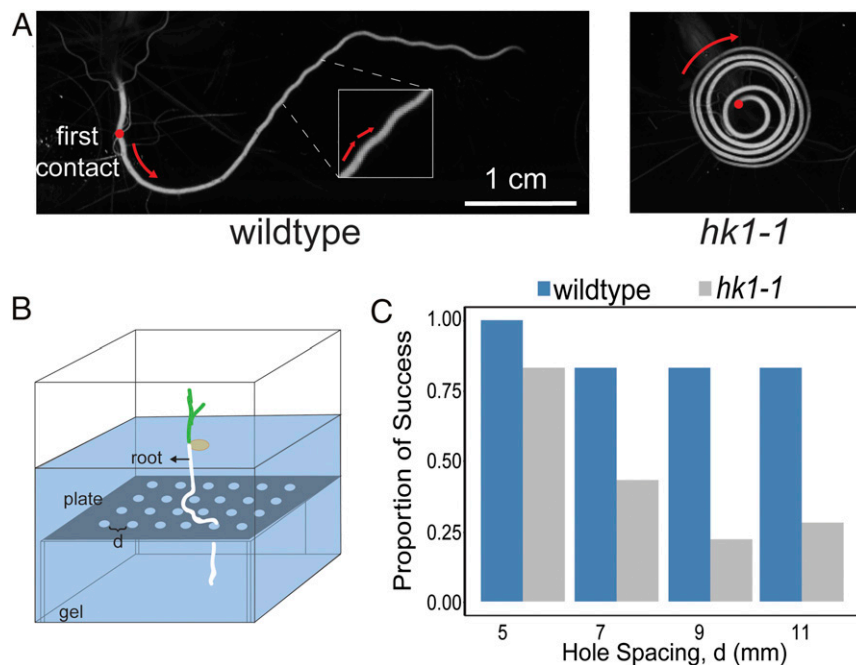


Fig. 4. *hkl1* has reduced surface exploration capacity. (A) Scan of bottom of growth container after wild-type and *hkl1-1* mutant primary roots struck a transparent solid surface. Red dots indicate the point of first contact with the surface, and red arrows represent direction of root growth. (B) Schematic of experimental setup to measure surface exploration. Platforms with holes separated by variable distances (d) were covered in gel-solidified media. Seeds were sown in the media and roots allowed to grow onto the platforms. (C) Quantification of success in growing through a hole for wild-type and *hkl1-1* mutant primary roots at different hole spacings. Fraction of success = 11/11, 10/12, 5/6, and 5/6 for wild type and 10/12, 7/16, 4/18, and 2/7 for *hkl1* at 5-, 7-, 9-, and 11-mm hole spacings, respectively.

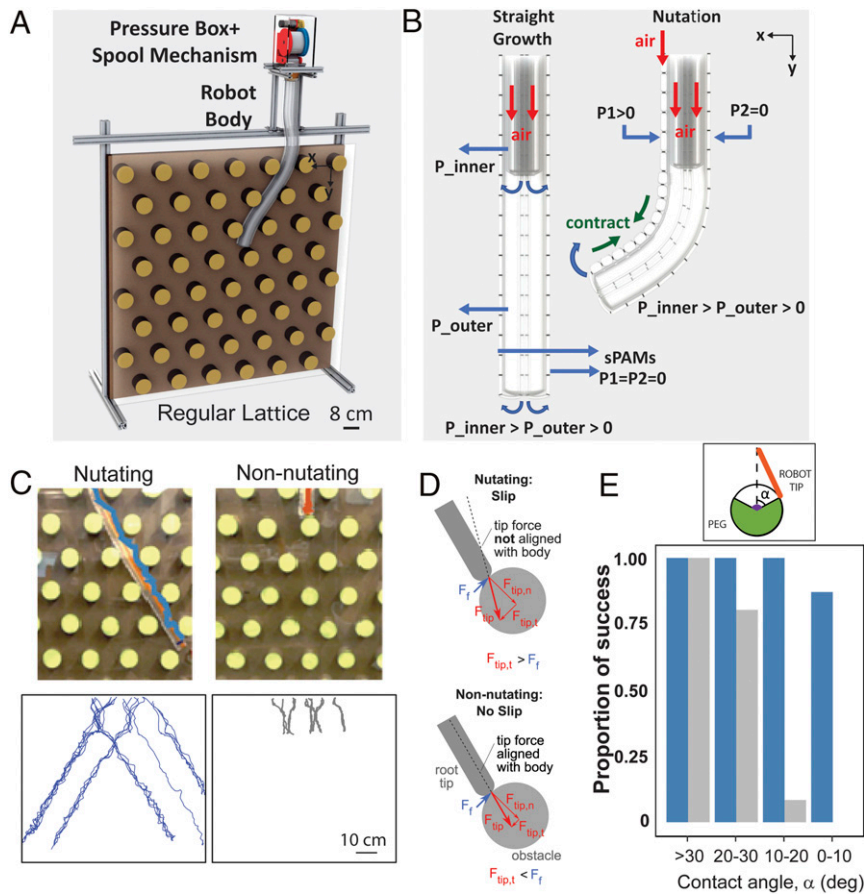


Fig. 5. Robophysical model of root growth in heterogeneous substrates. (A) Drawing of obstacle course and pneumatically actuated robotic root. The main body of the robot is attached to the pressure control box, and the spool mechanism simultaneously winds/unwinds the growing part of the robot during expansion/rewinding. (B) When the pressure of the inner body is greater than the pressure of the outer tip body and both are greater than zero gauge ($P_{\text{inner}} > P_{\text{outer}} > 0$), the robot grows with tip eversion. Only the lower pressure tip bends if one of the side actuators (sPAMs) is activated (P_1 or $P_2 > 0$). (C) (Top) Representative images of the robot at the most common growth length with (Left) and without (Right) nutation. (Bottom) Trajectories of nutating with a period of 5 s (blue, 21 experiments) and nonnutating (gray, 21 experiments) robot roots through the regular lattice of round pegs starting from the different initial positions. (D) For the nonnutating case, the tip force is aligned with the body; this means that the tangential component of the tip force ($F_{\text{tip,t}}$) is only created through misalignment of the tip with the obstacle. For nearly head-on collisions, $F_{\text{tip,t}}$ will be less than the force of friction, F_f , and no slip occurs. For the nutating case, the tip force is not always aligned with the body, and the oscillating lateral force means that $F_{\text{tip,t}}$ can exceed F_f to cause slip and passage of the obstacle. (E) The proportion of obstacles that the robot tip successfully passed with nutation (blue, 21 experiments with a total of $n = 17, 12, 15,$ and 15 contacts) and without nutation (gray, 21 experiments with $n = 7, 5, 12,$ and 9 contacts) in each contact angle range (α). The inset shows the contact angle when the tip (orange) hits the peg (green).

always stuck to the peg and could never grow farther (Fig. 5C and *SI Appendix*, Fig. S9). To derive a single measure of penetration effectiveness, we calculated the proportion of times any root struck a peg and was able to continue growing (*SI Appendix*, Fig. S9 and *Materials and Methods*). Overall, 97% of collisions of a nutating root with a peg resulted in a successful traversal, whereas only 36% of collisions by nonnutating roots resulted in a traversal (chi-squared test P value = 7.768×10^{-10} , *SI Appendix*, Fig. S9). These results indicate that a simple oscillatory motion may be sufficient for the emergence of improved root exploratory ability and are consistent with prior experimental and theoretical work demonstrating efficient exploration by plant-inspired circumnutating models (42–44).

The *hk1* Mutant Is Defective at Penetration of Clay Particles. Our platform experiment and robotic simulation suggest root exploration can be understood as a probabilistic process for which impenetrable obstacles along the growth path of the root represent potential failure points. This is consistent with the hypothesis that circumnutation is an adaptation to facilitate root penetration in soil containing dense heterogeneities, such as rocks or compaction. To test this hypothesis, we germinated wild-type and *hk1* mutant seeds

on irregularly shaped calcined clay gravel of a defined size distribution saturated with liquid growth media. This experiment models the situation encountered by the seeds of semiaquatic plant species such as rice adapted to germination in heterogeneous, water-logged soil conditions. We noted a striking phenomenon in which the roots of wild type would effectively burrow into the gravel layer, while mutant seedlings' roots often became caught near the surface, leading to dislodging of the seeds, rolling of the shoot downward, and aerial exposure of long root segments in protruding arcs (Fig. 6A and *Movie S9*). We quantified this effect by planting seeds of wild type and mutant on 1.5 cm of gravel overlaying a gel layer and counting the number of primary roots emerging into the gel layer 3 d postgermination (Fig. 6B and *Movie S10*). In this experiment, we observed 77% of wild-type roots penetrating into the gel layer but only 48% of mutant roots (chi-squared test P value = 0.000238, Fig. 6C). Thus, our robotic modeling of circumnutation accurately predicted the reduction in penetration ability of mutant roots in a heterogeneous growth substrate. The simulation, despite its simplicity, was able to capture an essential mechanical function of circumnutation. Collectively, these results indicate root circumnutation promotes seedling

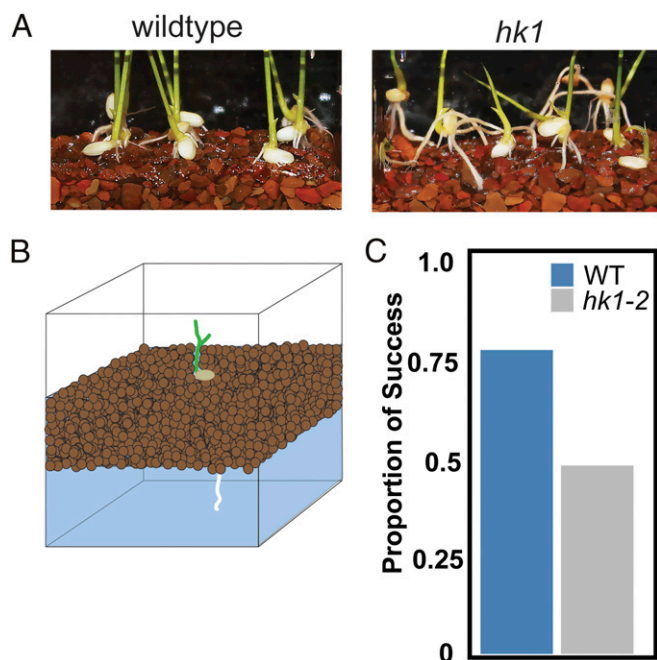


Fig. 6. *hk1* is defective in penetration of granular substrates. (A) Example root growth on liquid-saturated gravel surface for wild-type and *hk1* mutant primary roots. (B) Schematic of experimental setup to measure gravel penetration. (C) Quantification of success in growing through a 1.5-cm layer of gravel within 3 d of germination. $n = 88$ and 71 roots for wild type and *hk1-2*, respectively. Two-sided chi-squared test P value = 0.0001253.

establishment by aiding in effective exploration of dense, heterogeneous substrates.

Discussion

Our results provide support for a model in which *HK1* signaling positively regulates establishment of a mobile signal transported cell to cell in a helical, wave-like pattern, modulating cell elongation and producing circumnutation. Our genetic and physiological results suggest that the mobile signal is auxin given that circumnutation appears to require both auxin influx and efflux, and auxin is known to be directionally transported and regulate root cellular elongation. Our evidence suggests *HK1* regulates the influx step of auxin transport. It will be interesting to examine genetic regulators of auxin efflux during circumnutation.

Once circumnutation has been initiated, it appears to be employed by the root as a robust exploratory strategy. This is likely to be of critical importance to primary roots in natural growth settings, which emerge when the seed is unanchored. Searching for a path of least resistance into the soil is likely a preferable strategy to attempting concerted downward growth. This highlights a key conclusion from our study: There appears to be a tradeoff between rapid, unidirectional root elongation and multidimensional root exploration. We anticipate continued study of circumnutation will provide additional insight into regulation of exploratory root growth.

Materials and Methods

Plant Materials and Growth Conditions. The *hk1* mutants are in the KitaakeX background, a wild-type Kitaake line transformed with the *XA21* gene driven by the maize (*Zea mays*) ubiquitin promoter (12, 13). *oshk1-1* is from the mutant line FN-287 and has a single base substitution at position Chr6:26808461. *oshk1-2* is from FN-179 and has an inversion between Chr6:25948672 and 26809852. *oshk1-3* is from FN790-S and has a deletion from Chr6:26807814 to 26812817. Genomic coordinates are from Os-Nipponbare-Reference-IRGSP-1.0 (45). The

osaux1-3 mutant is in the Dongjin cultivar and contains a transfer DNA insertion in exon 6 (46).

Seeds were dehulled, sterilized with 50% bleach for 10 min, and rinsed four to five times with sterile water. All plant growth was in Yoshida's nutrient solution solidified with gellan gum [Gelzan, Caisson Inc. (47)].

For time-lapse imaging experiments, sterilized seeds were grown directly in GA-7 Magenta vessels containing media solidified with 0.15% Gelzan, except auxin treatment experiments in which plants were grown in sterilized, cut pipet tip racks supported by fiberglass mesh floating in liquid Yoshida's medium and the surface exploration experiment in which plants were grown in 0.5% gelzan solidified Yoshida's media. After planting, seeds were incubated for 2 d in the dark at 30 °C; vessels were then moved to constant low light (~650 lx) at 22 to 23 °C for imaging, except the surface exploration experiment, which was conducted under 12-h light/dark cycles with nighttime illumination when the camera imaged each shelf.

Time-Lapse Imaging. We designed and constructed two robotic automatic imaging systems to acquire images of rice plants growing in Magenta containers at 15-min intervals. The robot was capable of simultaneously imaging 100 and 85 containers, respectively. FLIR Flea3 cameras (FL3-U3-1352C-CS or FL3-U3-1352M-CS) were positioned facing the front of the growth containers to visualize root tip circumnutation and root depth. The cameras were moved at set intervals by Arduino-controlled horizontal and vertical gantries (universal product code 819368022278, OpenBuilds) with NEMA 17 stepper motors (universal product code 819368021264 and 819368021226, OpenBuilds). Illumination was provided by light-emitting diode strip lights (Novostella, B075RYSHQQ).

Analysis of Primary Root Length. The lengths of the primary roots from a sample of wild type and *hk1-1*, *hk-2*, and *hk1-3* were calculated by measuring the roots from photographs of the respective genotypes 2 d postgermination. Germination was defined as the point when the primary root had emerged and grown to a depth equal to the bottom of the seed. An analysis script, along with the raw data, has been included in *SI Appendix, Dataset S1*.

Statistical Analysis of Primary Root Length. We performed two-sided Wilcoxon Rank Sum tests comparing wild-type and mutant primary root lengths. A script performing this procedure, along with raw data, has been included in *SI Appendix, Dataset S1*.

Root Tip Tracing. Root tip tracing was performed by marking the position of the root tip in successive images in ImageJ. These coordinates were input into R, and an estimated central axis of root growth was calculated using loess regression. We then calculated the distance of the root tip from this central axis of root growth at each time point and fit a highly flexible natural cubic spline model using the splines package in R in order to visualize the path of the root tip. Conversion from pixel to distance was accomplished by calculating a conversion factor derived from an image of a standard metric ruler placed at the same distance from the camera as the roots typically grow. A script performing these functions, along with raw data, has been included in *SI Appendix, Dataset S2*.

Circumnutation Amplitude Quantification. For quantification of circumnutation amplitude for wild-type KitaakeX versus *hk1*, wild-type KitaakeX \pm 1-MCP, *hk1* \pm cytokinin, wild-type KitaakeX \pm NPA, and wild-type Dongjin versus *aux1*, we modified the above script to identify local extrema in the measurements of root tip displacement within an 8-h window after circumnutation that had increased to a maximum amplitude in the given condition. In wild-type KitaakeX and Dongjin, we found circumnutation was at or near maximum amplitude 40 to 48 h after germination, and in cytokinin-treated *hk1* mutant, we found it occurred between 50 and 58 h after germination. We then averaged the displacement of the root tip from the central axis of growth at each local extremum during this time window to calculate an average circumnutation amplitude and compared it to the negative control over the same time frame. In the 1-MCP experiment, we allowed roots to grow for ~2 d and then treated with 1-MCP. We measured circumnutation amplitude in the time period 2 to 10 h after addition. A similar procedure was performed for *hk1* \pm 1-NAA, except because of the extreme reduction in root elongation rate observed after 1-NAA treatment, we instead averaged the four final local extrema observed during the ~24 h of imaging with the hormone (two maxima and two minima).

Statistical Analysis of Circumnutation Amplitude. We performed two-sided Wilcoxon Rank Sum tests comparing control and test condition

circumnutation amplitudes in each respective experiment. A script performing this procedure, along with raw data, has been included in *SI Appendix, Dataset S3*.

Root Cell Length Measurements. Roots of 2- to 3-d-old seedlings were assayed for cell length measurements. In wild type, circumnating roots were defined as those with at least 15° bending of the root tip. Roots were live stained with 1 mg/mL calcofluor white or 10 mg/mL propidium iodide for 5 min and immediately imaged using a Zeiss 510 or Zeiss 880 confocal microscope. A combined tile scan/z-stack of the root tip and elongation zone of the roots was used to capture overall root shape and cell structure. In ImageJ, a line perpendicular to the direction of root growth was used to mark the region of the root exhibiting maximal bending. We then measured the longitudinal cell length at the region of maximal bending for 15 epidermal cells on the inner and outer flanks of the root (nine cells rootward, five cells shootward, and one cell at the position of maximum bending). We then took the difference of the total length of the 15 cells on the outer and inner bend, the result of which is plotted in Fig. 1E. For the mutant, we performed the same procedure, making a line at ~1 mm from the root tip and measuring cells on both sides of the root before arbitrarily subtracting the length of the measured cells from one side of the root from the length of the cells on the other.

Statistical Analysis of Root Cell Length. We performed a two-sided Wilcoxon Signed Rank test comparing the difference in 15-cell length from one side of the root to the other under the null hypothesis that they are centered on zero. A script performing this procedure, along with raw data, has been included in *SI Appendix, Dataset S4*.

Hormone Treatment/Inhibitor Experiments. For the 1-MCP experiment, we grew seeds of wild type in magenta boxes, as above, and ~2 d after germination when circumnutation had been strongly initiated, we added freshly prepared 0.014% 1-MCP mixed with 1 mL water sufficient to fill a 300-mL box to a concentration of 5 μL/L (EthylBloc, AgroFresh). We then tightly sealed the lids of the boxes with parafilm. For cytokinin treatment experiments, 150 μM stock *trans*-zeatin in 0.01 N KOH was added to autoclaved media to create 150 nM working concentration (Sigma, Z0876). For the NPA experiment, 50 mM stock NPA in DMSO was first diluted in sterile water and added to autoclaved media to create a final concentration of 40 nM (Sigma, 33371). An equivalent amount of DMSO was used for the negative control. A total of 200 mM IAA in ETOH was first diluted in sterile water and then added to hydroponically growing rice roots ~1 d after germination to create a final concentration of 200 nM (GoldBio, I-110-25). A total of 200 mM 1-NAA and 2-NAA stock solutions in acetone were diluted in sterile water and added to hydroponically grown rice roots ~1 d after germination to create a final concentration of 200 nM (Sigma, N0640 and N4002).

RNA-Sequencing. Single 2-mm root tip sections were isolated from 2 d postgermination seedlings. Sections were initially harvested into 10 μL RNA-later (Ambion) in the lid of a 2-mL screw cap homogenization tube. A total of 200 μL Tri-Reagent (Zymo) was added to the tube, along with two 3-mm stainless-steel grinding balls, and the cap containing the tissue section was closed on the tube. It was inverted several times to wash the tissue section into the Tri-Reagent. Samples were frozen in liquid nitrogen and stored at -80 and then processed by grinding with a bead homogenizer with 30-s pulses, 1,500 Hz, until the Tri-Reagent thawed (three to four cycles). RNA was isolated using the Zymo MagBead RNA Isolation kit according to manufacturer's protocol (Zymo). A total of 100 to 200 ng RNA was used as input into the QuantSeq 3' FWD RNA-Seq library preparation procedure according to the manufacturer's protocol, using the Unique Molecular Identifier (UMI) PCR add-on kit (Lexogen). Libraries were indexed and pooled one lane of Illumina NextSeq, High Output setting. Reads were aligned to Michigan State University Rice genome version 7 using the STAR aligner (48), deduplicated using UMI-Tools (49), and counted with HTSeq-Count. Counts were analyzed with edgeR (50). We defined "expressed genes" to be those with observed reads in three or more libraries. Files containing processed counts-per-million are included in *SI Appendix, Dataset S5*, and raw reads have been deposited at the Sequence Read Archive (SRA) under BioProject ID PRJNA615381.

Platform Exploration Assay. Seeds were sown in Magenta vessels containing media solidified with 0.5% Gelzan. Containers had raised polycarbonate surfaces of equal height with holes of 2.5-mm diameter equally spaced in a square grid at distances of 5, 7, 9, and 11 mm. Plants were grown on a robotic imaging system. We modified the robot by adding a second camera

oriented at a 45° angle downward to visualize the growth of the roots on the platforms.

The containers were imaged for a minimum period of 5 d. A trial was considered a success when the primary root hit a surface and found a hole within 72 h of first hitting the surface; failures occurred when the root hit the surface but did not find a hole in that time period. Exclusions included trials in which the plant had no primary roots, the primary root never hit the surface or directly found the hole without surface contact, the primary root grew out of view of the camera, or the growth media was visibly contaminated.

Statistical Analysis of Platform Exploration Assay. There were 11, 12, 6, and 6 roots of wild type and 12, 16, 18, and 7 roots of mutant allowed to grow on a platform for 72 h at hole spacings of 5, 7, 9, and 11 mm, respectively. "Success" was defined as the root tip encountering and growing into a hole. We modeled the probability of success using logistic regression with hole spacing and genotype as covariates. Based on the Wald test, we observed effects of genotype and spacing with *P* values = 0.000211 and 0.007853, respectively. We utilized Wald-based CI estimation to determine CIs for the odds ratios (95% CI for odds ratio for genotype: 3.43, 45.09; 95% CI for spacing: 0.4966817, 0.8628481). An analysis script, along with raw data, has been included in *SI Appendix, Dataset S6*.

Robotic Root Design. To generate 2D oscillation at the tip, we used two series pneumatic artificial muscles [sPAMs (39, 40)] attached to the left and right side of the main body (Fig. 5B). The sPAMs include multiple pouch motors (51) that are made of lay-flat poly tubing (*d*_{tube} = 25 mm) with O-rings (*d*_{ring} = 4.5 mm) spaced at 2-cm intervals. When the sPAMs are inflated, the segments separated by O-rings extend radially and shorten longitudinally. The shortening length of the sPAM bends the tip of the robot to the corresponding side. A key innovation is our method of localizing oscillation to only the tip. In ref. 39, the entire body bends when a sPAM is actuated. To achieve tip-only oscillation, we incorporate a second internal growing body inside the main growing outer body. This internal body grows at the same rate as the outer body but is shorter and at a higher pressure. In this manner, the tip of the robot is formed by the outer body only and is thus at a lower pressure than the rest of the body. Therefore, when a sPAM is actuated, only the lower pressure tip bends.

Robotic Root Peg Assay. The robotic root was tested in an obstacle course to examine the exploratory capabilities of the nutation behavior. Peg obstacles were placed in a triangular lattice as described in ref. 40. A transparent plastic sheet kept the robot root constrained to the 2D plane of obstacles.

Definition of Robot Root Contact. To measure the effectiveness of obstacle traversal, we analyzed what occurred after the robot tip first hit an obstacle. The touch of the robot tip was considered "hitting" if the angle (α) between the line that connects the tip to the center of a peg and the line passing from the center of a peg to the center of the root ~15 cm away is less than ~60° (*SI Appendix, Fig. S9*). *SI Appendix, Fig. S9* shows two snapshots from the experiment; the left panel shows an example of "hitting," and the right panel shows an example of contact not labeled as "hitting."

Peg Interaction Measurements. We performed two sets of experiments (21 experiments per each case) on the regular obstacle lattice, with a period of 5 s and without tip oscillation starting from different initial conditions. The horizontal starting position of the robot was changed in ±6-cm increments up to ±25 cm distance from the center of the upper edge of the lattice. At each initial condition, we performed three experiments. We tracked the robot tip from the video frames (one frame per second) using MATLAB.

We counted the total number of times each root hit an obstacle before either becoming stuck or reaching the maximum extrusion length of about 1 m. To estimate an overall metric of obstacle traversal effectiveness, we counted the total number of times any root hit an obstacle and successfully grew beyond. We divided this number by the total number times any root hit an obstacle.

Peg Angle Measurements. We analyzed each interaction of the root with a peg and measured the angle of the root, as defined above, and whether the interaction resulted in a traversal or immobilization for both nutating and nonnutating roots.

Statistical Analysis of Peg Interaction. A chi-squared test for independence was performed on the 2 × 2 contingency table corresponding to the successes and failures of the nutating and nonnutating robotic root in growing

past an obstacle. An analysis script, along with raw data, has been included in *SI Appendix, Dataset S7*.

Gravel Exploration Assay. Seeds were surface sterilized and pregerminated for 1 d in sterile liquid media at 30 degrees celsius in the dark before being surface sown onto a 1.5-cm layer of liquid saturated autoclaved calcined clay gravel (Turface MVP, percent retained at mesh size 3.36 mm, 16.4% ± 5.0%; 2.38 mm, 41.1% ± 5.4%; 1.68 mm, 23.7% ± 3.5%; and 0.841 mm, 18.0% ± 6.6%) on top of a 100-mL volume of 0.15% gelatin solidified Yoshida's media inside magenta boxes, with nine seeds total per box. These boxes were imaged in the automated robotic imaging system for 4 d. We defined 1 d post-sowing as germination and then counted the number of roots emerging from the gravel layer into the gel layer 3 d later. This quantity gave the numerator for our calculation of the proportion of success. We calculated the denominator by counting the number of seeds that had germinated with an emerged primary root. We planted a total of 11 boxes of both wild type and mutant, with a total of 88 and 71 germinating wild-type and mutant seeds, respectively.

Statistical Analysis of Gravel Exploration. A chi-squared test for independence was performed on the 2 × 2 contingency table corresponding to the successes and failures of the wild-type and *hk1-2* roots growing into the gel layer 3 d after germination. An analysis script, along with raw data, has been included in *SI Appendix, Dataset S8*.

Video Processing. For plant growth, time-lapse movies were created with ffmpeg at a framerate of 15 frames/s (FFmpeg Project), except for the platform experiment for which the video was created in MATLAB at 10 frames per

second. Since images were taken every 15 min, this translates to 225 min growth/1 s of video (or 150 min growth/second in the platform video). Videos were stabilized and brightness/contrast adjusted with Premiere Pro-2019 (Adobe). In some videos, masks were applied along the edge of the video to occlude roots from adjacent plants growing into the field of view. In other cases, masks were applied to portions of the field of view unconnected to the seed or root where blemishes in the box created small regions of scattered light. Aside from stabilization and brightness/contrast adjustment, the region of the movie occupied by the seed or root was not modified.

Data Availability. RNA-Seq (datasets and code to reproduce statistical analyses) data have been deposited in the Duke Research Data Repository (<https://doi.org/10.7924/r4b27x11m>), and raw reads have been deposited at Sequence Read Archive under BioProject ID PRJNA615381. All other study data are included in the article and/or *SI Appendix*.

ACKNOWLEDGMENTS. This work was supported by a grant from the NSF (NSF PHY-1915445) to D.I.G. and P.N.B., by a NSF Graduate Research Fellowship to K.R.L., by the Howard Hughes Medical Institute and the Gordon and Betty Moore Foundation (through Grant GBMF3405) to P.N.B., by the Dunn Family Professorship to D.I.G. and E.N.M., and U.S. NSF (Award #1237975), the Foundation for Food and Agricultural Research (Award #534683), and the NIH (GM122968) to P.C.R. We thank Medhavinee Mijar, Carrie Hunner, Milan Shah, Enes Aydin, and Anupam Mijar for assistance in collecting and analyzing data, the staff of the Duke Phytotron for plant care, the Duke Center for Genomic and Computational Biology for Illumina sequencing services, and Drs. Lucia Strader, Sabrina Sabbatini, Jazz Dickinson, Trevor Nolan, Edith Pierre-Jerome, and Pablo Szekely for critical reading of the manuscript as well as Drs. Joe Kieber and Flor Ercoli for helpful discussions.

1. A. G. Bengough, B. M. McKenzie, P. D. Hallett, T. A. Valentine, Root elongation, water stress, and mechanical impedance: A review of limiting stresses and beneficial root tip traits. *J. Exp. Bot.* **62**, 59–68 (2011).
2. L. Clark, W. Whalley, P. Barraclough, "How do roots penetrate strong soil?" in *Roots: The Dynamic Interface between Plants and the Earth*, J. Abe Ed. (Springer, New York, NY, 2003), pp. 93–104.
3. M. Campbell, F. Swain, Effect of strength, till and heterogeneity of the soil surface on radicle-entry of surface-sown seeds. *Grass Forage Sci.* **28**, 41–50 (1973).
4. P. M. Dowling, R. J. Clements, J. R. McWilliam, Establishment and survival of pasture species from seeds sown on the soil surface. *Aust. J. Agric. Res.* **22**, 61–74 (1971).
5. J. Schutzen, J. Dainty, A. J. Davy, Root anchorage and its significance for submerged plants in shallow lakes. *J. Ecol.* **93**, 556–571 (2005).
6. P. Perona *et al.*, Biomass selection by floods and related timescales: Part 1. Experimental observations. *Adv. Water Resour.* **39**, 85–96 (2012).
7. B. Crouzy, P. Perona, Biomass selection by floods and related timescales. Part 2: Stochastic modeling. *Adv. Water Resour.* **39**, 97–105 (2012).
8. C. Darwin, *The Power of Movement in Plants*, F. Darwin, Ed. (Cambridge University Press, 1880).
9. N. Inoue *et al.*, Ecological significance of root tip rotation for seedling establishment of *Oryza sativa* L. *Ecol. Res.* **14**, 31–38 (1999).
10. Y. Hayashi *et al.*, An aluminum influence on root circumnutation in dark revealed by a new super-HARP (high-gain avalanche rushing amorphous photoconductor) camera. *Plant Cell Physiol.* **45**, 351–356 (2004). Correction in *Plant Cell Physiol.*, **22**, 501 (2004).
11. G. Li *et al.*, Genome-wide sequencing of 41 rice (*Oryza sativa* L.) mutated lines reveals diverse mutations induced by fast-neutron irradiation. *Mol. Plant* **9**, 1078–1081 (2016).
12. G. Li *et al.*, The sequences of 1504 mutants in the model rice variety Kitaake facilitate rapid functional genomic studies. *Plant Cell* **29**, 1218–1231 (2017).
13. R. Jain *et al.*, Genome sequence of the model rice variety KitaakeX. *BMC Genomics* **20**, 905 (2019).
14. C. N. Topp *et al.*, 3D phenotyping and quantitative trait locus mapping identify core regions of the rice genome controlling root architecture. *Proc. Natl. Acad. Sci. U.S.A.* **110**, E1695–E1704 (2013).
15. A. S. Iyer-Pascuzzi *et al.*, Imaging and analysis platform for automatic phenotyping and trait ranking of plant root systems. *Plant Physiol.* **152**, 1148–1157 (2010).
16. H. Takehisa *et al.*, Genome-wide transcriptome dissection of the rice root system: Implications for developmental and physiological functions. *Plant J.* **69**, 126–140 (2012).
17. S.-H. Su, N. M. Gibbs, A. L. Jancewicz, P. H. Masson, Molecular mechanisms of root gravitropism. *Curr. Biol.* **27**, R964–R972 (2017).
18. S. Piconese, G. Tronelli, P. Pippia, F. Migliaccio, Chiral and non-chiral mutations in *Arabidopsis* roots grown on the random positioning machine. *J. Exp. Bot.* **54**, 1909–1918 (2003).
19. F. Migliaccio, P. Tassone, A. Fortunati, Circumnutation as an autonomous root movement in plants. *Am. J. Bot.* **100**, 4–13 (2013).
20. R. T. Clark *et al.*, Three-dimensional root phenotyping with a novel imaging and software platform. *Plant Physiol.* **156**, 455–465 (2011).
21. H. Zhao *et al.*, Histidine kinase MHZ1/OsHK1 interacts with ethylene receptors to regulate root growth in rice. *Nat. Commun.* **11**, 518 (2020).
22. Y.-C. Tsai *et al.*, Characterization of genes involved in cytokinin signaling and metabolism from rice. *Plant Physiol.* **158**, 1666–1684 (2012).
23. M. Adamowski, J. Friml, PIN-dependent auxin transport: Action, regulation, and evolution. *Plant Cell* **27**, 20–32 (2015).
24. R. Swarup, R. Bhosale, Developmental roles of AUX1/LAX auxin influx carriers in plants. *Front Plant Sci* **10**, 1306 (2019).
25. H.-j. Kim, A. Kobayashi, N. Fujii, Y. Miyazawa, H. Takahashi, Gravitropic response and circumnutation in pea (*Pisum sativum*) seedling roots. *Physiol. Plant.* **157**, 108–118 (2016).
26. E. P. Maher, S. J. B. Martindale, Mutants of *Arabidopsis thaliana* with altered responses to auxins and gravity. *Biochem. Genet.* **18**, 1041–1053 (1980).
27. K. Okada, Y. Shimura, Reversible root tip rotation in *Arabidopsis* seedlings induced by obstacle-touching stimulus. *Science* **250**, 274–276 (1990).
28. C. Simmons, D. Söll, F. Migliaccio, Circumnutation and gravitropism cause root waving in *Arabidopsis thaliana*. *J. Exp. Bot.* **46**, 143–150 (1995).
29. C. Garbers, A. DeLong, J. Deruère, P. Bernasconi, D. Söll, A mutation in protein phosphatase 2A regulatory subunit A affects auxin transport in *Arabidopsis*. *EMBO J.* **15**, 2115–2124 (1996).
30. J. L. Mullen *et al.*, Root-growth behavior of the *Arabidopsis* mutant rgr1. Roles of gravitropism and circumnutation in the waving/coiling phenomenon. *Plant Physiol.* **118**, 1139–1145 (1998).
31. G. D. Massa, S. Gilroy, Touch modulates gravity sensing to regulate the growth of primary roots of *Arabidopsis thaliana*. *Plant J.* **33**, 435–445 (2003).
32. A. A. Santner, J. C. Watson, The WAG1 and WAG2 protein kinases negatively regulate root waving in *Arabidopsis*. *Plant J.* **45**, 752–764 (2006).
33. M. V. Thompson, N. M. Holbrook, Root-gel interactions and the root waving behavior of *Arabidopsis*. *Plant Physiol.* **135**, 1822–1837 (2004).
34. A. Delbarre, P. Muller, V. Imhoff, J. Guern, Comparison of mechanisms controlling uptake and accumulation of 2,4-dichlorophenoxy acetic acid, naphthalene-1-acetic acid, and indole-3-acetic acid in suspension-cultured tobacco cells. *Planta* **198**, 532–541 (1996).
35. J. Dindas *et al.*, Pitfalls in auxin pharmacology. *New Phytol.* **227**, 286–292 (2020).
36. C. Yu *et al.*, The auxin transporter, OsAUX1, is involved in primary root and root hair elongation and in Cd stress responses in rice (*Oryza sativa* L.). *Plant J.* **83**, 818–830 (2015).
37. J. Giri *et al.*, Rice auxin influx carrier OsAUX1 facilitates root hair elongation in response to low external phosphate. *Nat. Commun.* **9**, 1408 (2018). Correction in *Nat. Commun.* **9**, 1810 (2018).
38. A. Marchant *et al.*, AUX1 regulates root gravitropism in *Arabidopsis* by facilitating auxin uptake within root apical tissues. *EMBO J.* **18**, 2066–2073 (1999).
39. J. D. Greer, T. K. Morimoto, A. M. Okamura, E. W. Hawkes, "Series pneumatic artificial muscles (SPAMs) and application to a soft continuum robot" in 2017 IEEE International Conference on Robotics and Automation (ICRA) (IEEE, 2017), pp. 5503–5510.
40. Y. Ozkan-Aydin *et al.*, "Nutation aids heterogeneous substrate exploration in a robotic root" in 2019 2nd IEEE International Conference on Soft Robotics (RoboSoft) (IEEE, 2019), pp. 172–177.
41. J. Aguilar *et al.*, A review on locomotion robophysics: The study of movement at the intersection of robotics, soft matter and dynamical systems. *Rep. Prog. Phys.* **79**, 110001 (2016).
42. E. Del Dottore, A. Mondini, A. Sadeghi, V. Mattoli, B. Mazzolai, An efficient soil penetration strategy for explorative robots inspired by plant root circumnutation movements. *Bioinspir. Biomim.* **13**, 015003 (2017).
43. F. Tedone, E. Del Dottore, M. Palladino, B. Mazzolai, P. Marcati, Optimal control of plant root tip dynamics in soil. *Bioinspir. Biomim.* **15**, 056006 (2020).

44. M. Wooten, C. Frazelle, I. D. Walker, A. Kapadia, J. H. Lee, "Exploration and inspection with vine-inspired continuum robots" in 2018 IEEE International Conference on Robotics and Automation (ICRA) (IEEE, 2018), pp. 1–5.
45. Y. Kawahara *et al.*, Improvement of the *Oryza sativa* Nipponbare reference genome using next generation sequence and optical map data. *Rice (N. Y.)* **6**, 4 (2013).
46. H. Zhao *et al.*, OsAUX1 controls lateral root initiation in rice (*Oryza sativa* L.). *Plant Cell Environ.* **38**, 2208–2222 (2015).
47. J. Cock, S. Yoshida, D. A. Forno, K. A. Gomez, *Laboratory Manual for Physiological Studies of Rice* (Int. Rice Res. Inst., ed. 3, 1976).
48. A. Dobin *et al.*, STAR: Ultrafast universal RNA-seq aligner. *Bioinformatics* **29**, 15–21 (2013).
49. T. Smith, A. Heger, I. Sudbery, UMI-tools: Modeling sequencing errors in unique molecular identifiers to improve quantification accuracy. *Genome Res.* **27**, 491–499 (2017).
50. M. D. Robinson, D. J. McCarthy, G. K. Smyth, edgeR: A Bioconductor package for differential expression analysis of digital gene expression data. *Bioinformatics* **26**, 139–140 (2010).
51. R. Niiyama *et al.*, Pouch motors: Printable soft actuators integrated with computational design. *Soft Robot.* **2**, 59–70 (2015).



Supplementary Information for

Title: Mechanism and function of root circumnutation

Authors: Isaiah Taylor, Kevin Lehner, Erin McCaskey, Niba Nirmal, Yasemin Ozkan-Aydin, Mason Murray-Cooper, Rashmi Jain, Elliot W. Hawkes, Pamela C. Ronald, Daniel I. Goldman, Philip N. Benfey

Corresponding author: Philip N. Benfey
Corresponding author email: philip.benfey@duke.edu

This PDF file includes:

Figures S1 to S10
Legends for Movies S1 to S10
Legends for Datasets S1 to S8

Other supplementary materials for this manuscript include the following:

Movies S1 to S10
Datasets S1 to S8

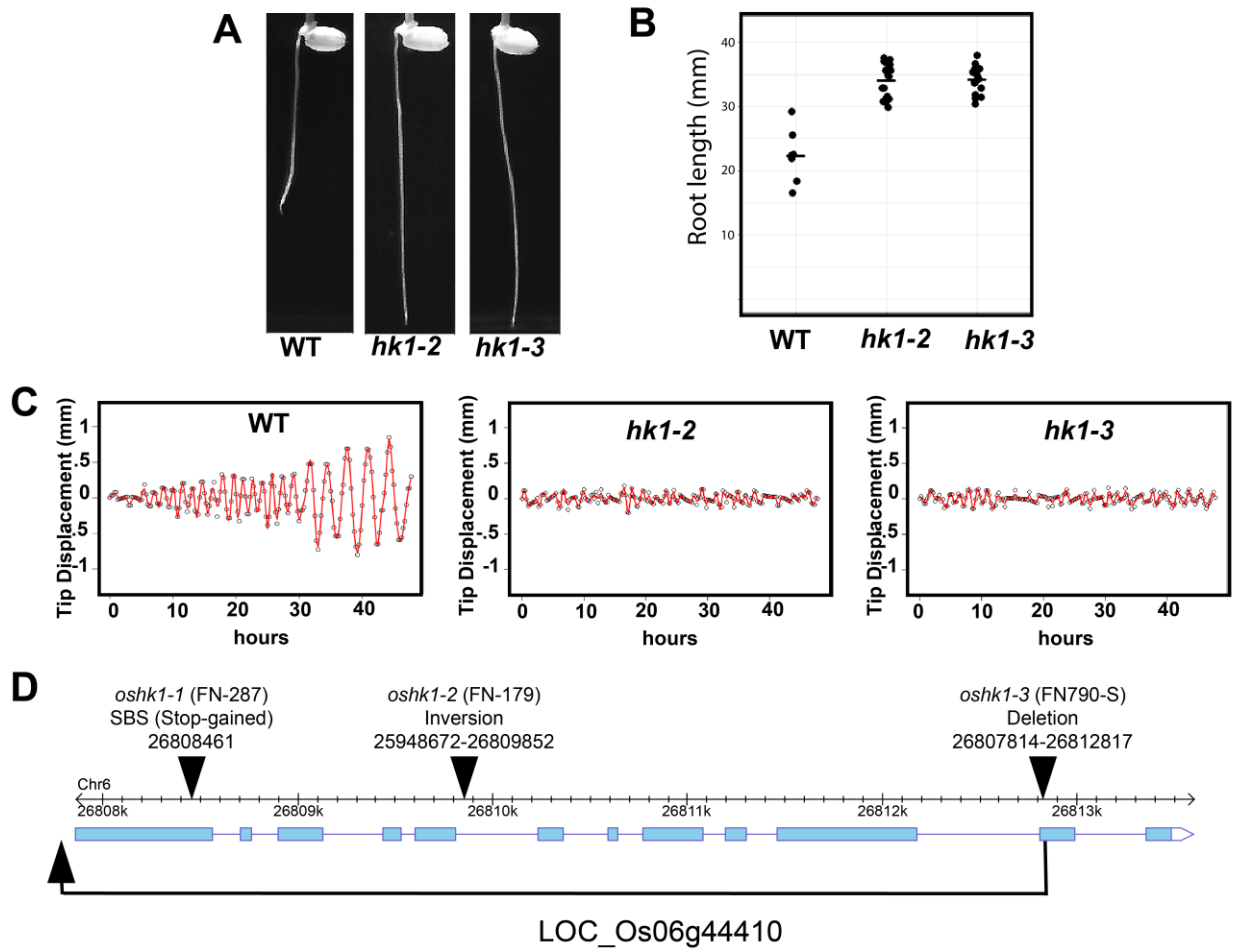


Fig. S1) Identification of allelic mutants of *hkl1* with identical deeper primary root depth and circumnutation phenotypes.

- A) Primary root growth of wildtype, *hkl1-2*, and *hkl1-3* 48 hours after germination
- B) Quantification of primary root length comparing wildtype to *hkl1-2* and *hkl1-3*.
- C) Tip traces of representative roots for wildtype, *hkl1-2*, and *hkl1-3* over 48 hours of growth
- D) Diagram of mutations in *hkl1-1*, *hkl1-2*, and *hkl1-3*.

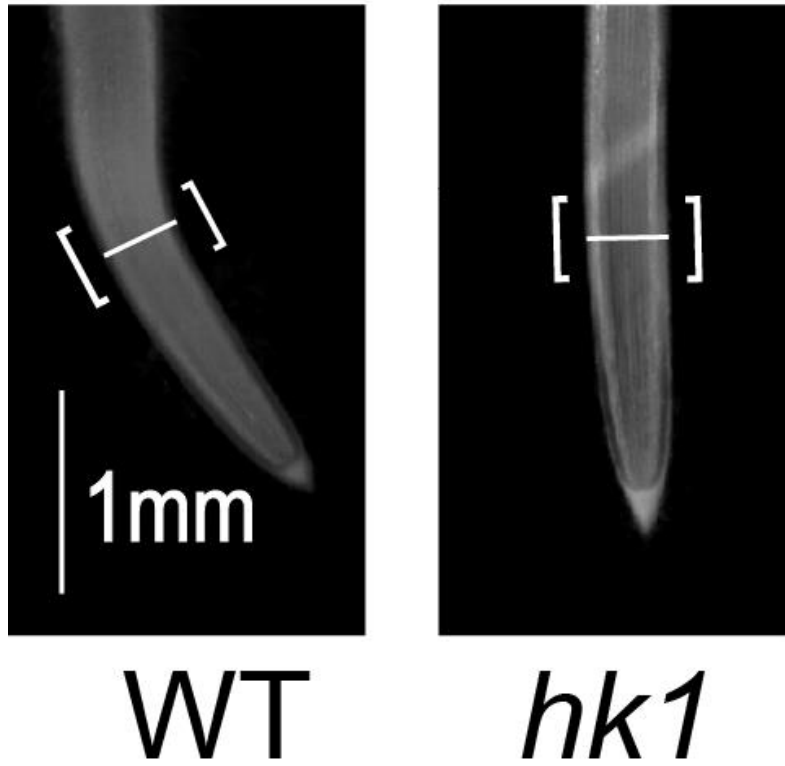
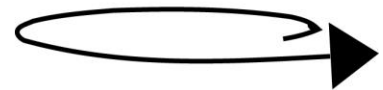
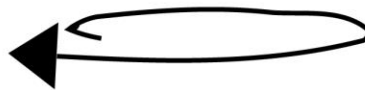


Fig. S2) Region of cell length measurements in wildtype and mutant.

A



B



Direction of rotation:

Clockwise

Counterclockwise

Proportion of wild-type roots: 11/21

10/21

Fig. S3) Maximum intensity projections of wild-type primary root growth

A) A root exhibiting clockwise rotation

B) A root exhibiting counterclockwise rotation

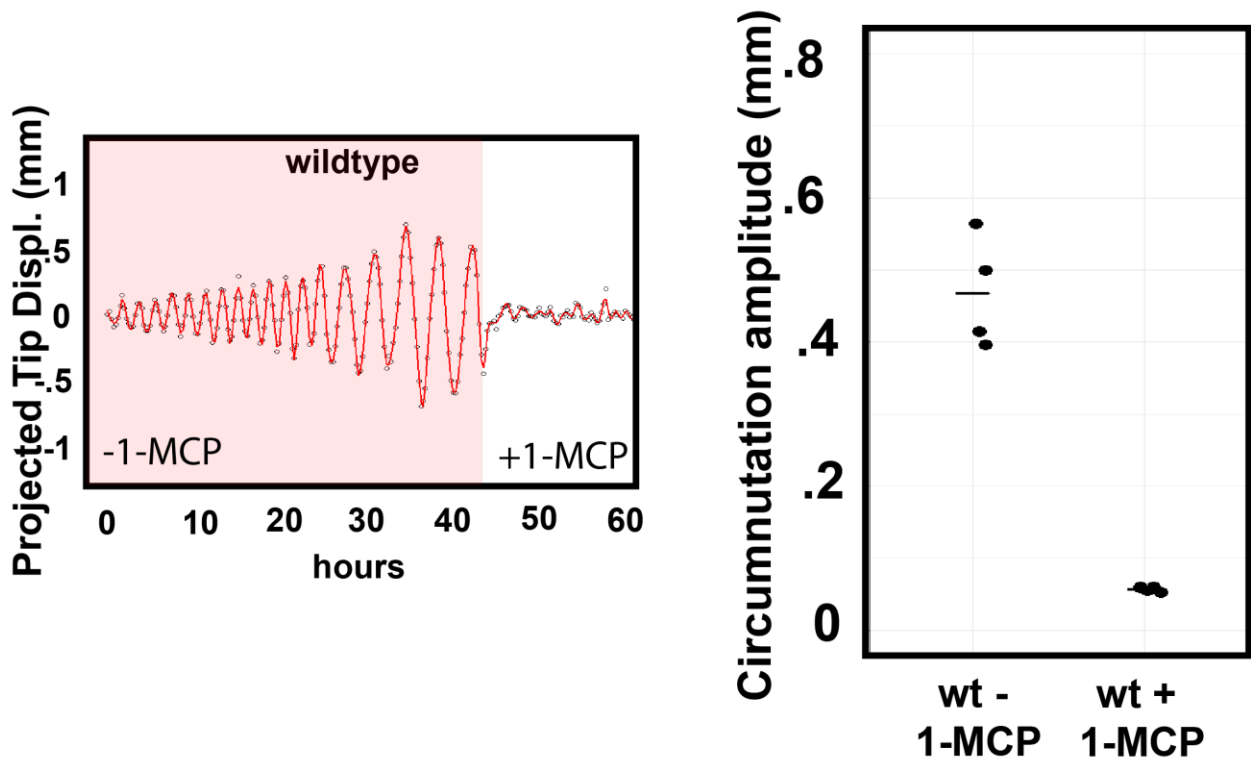


Fig. S4) Treatment of wildtype with the ethylene receptor inhibitor 1-MCP blocks circumnutation. Graph displays average amplitude of circumnutation after time-point of 1-MCP addition for 4 and 5 untreated and treated roots, respectively. Two-sided Wilcoxon rank-sum test p-value = 0.01587. Horizontal dash indicates mean value.

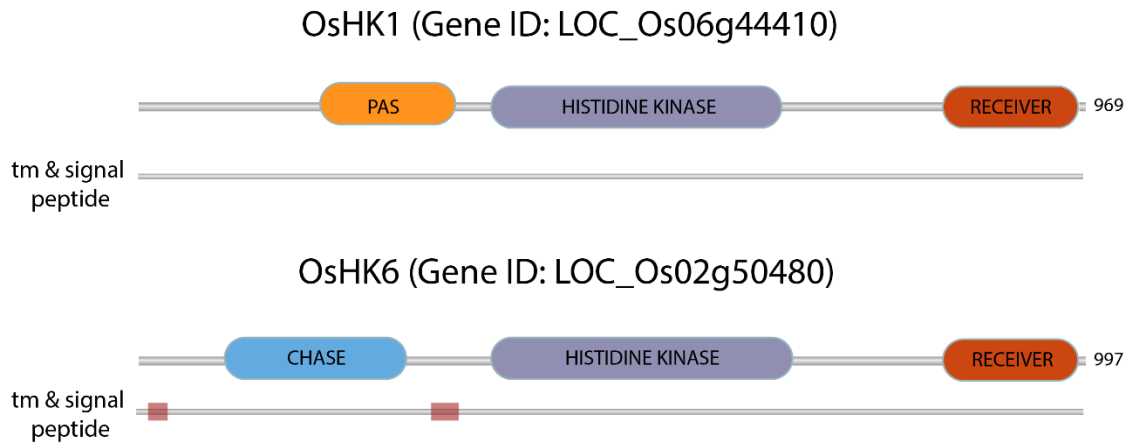


Fig. S5) Domain architecture of HK1 and a predicted canonical cytokinin receptor, HK6.

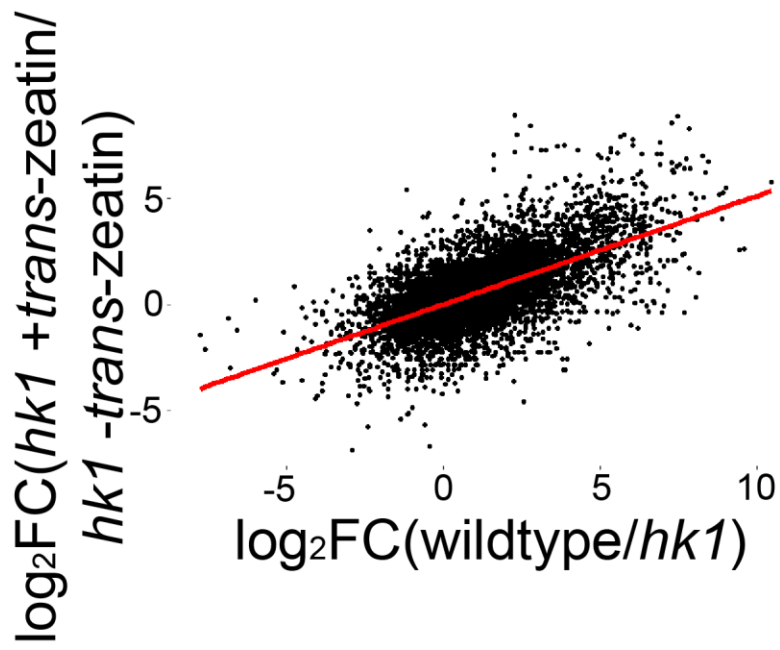


Fig. S6) $\log_2(\text{fold change})$ values for all genes in wildtype/*hk1* compared with *hk1* plus/minus *trans-zeatin*

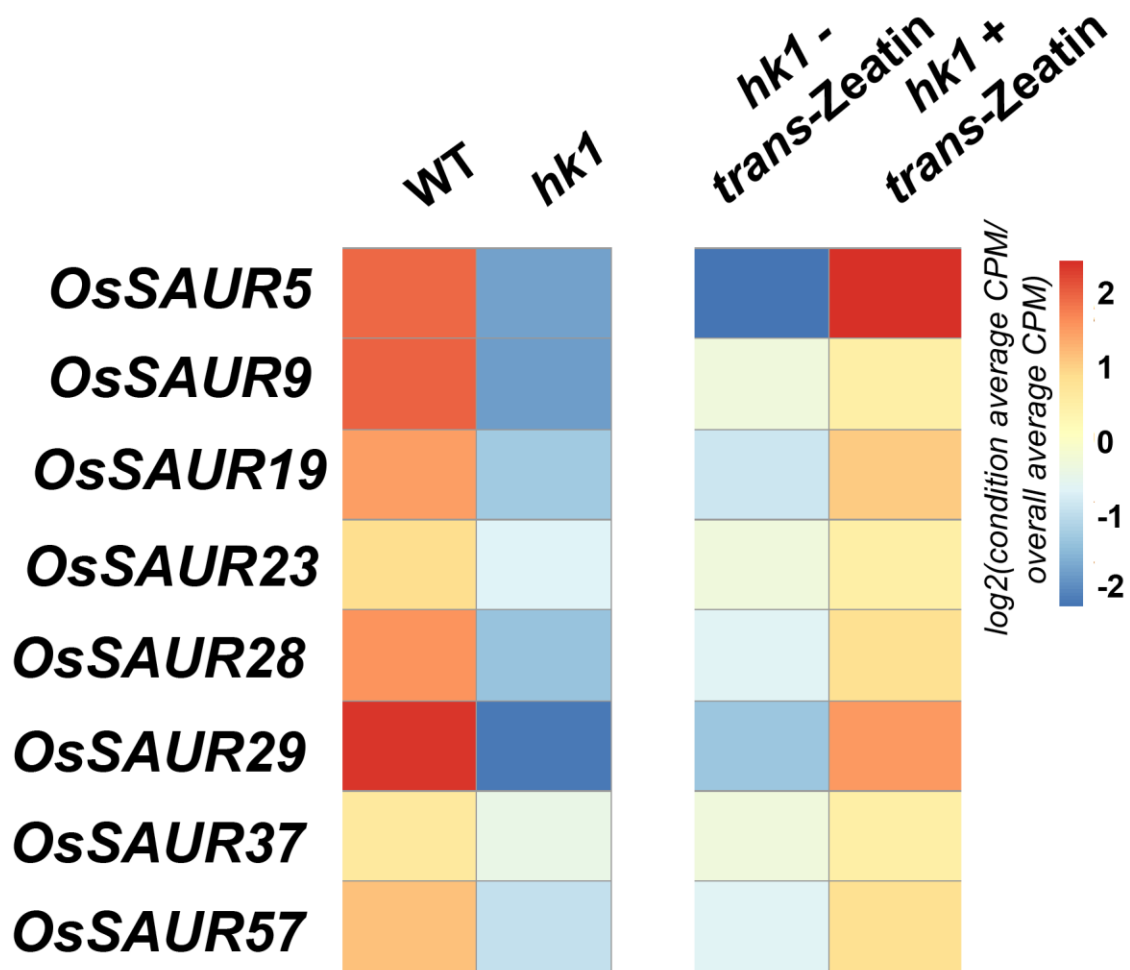


Fig. S7) log₂(fold change) of 8 differentially expressed SAUR genes for wildtype/*hk1* and *hk1* plus/minus *trans*-zeatin

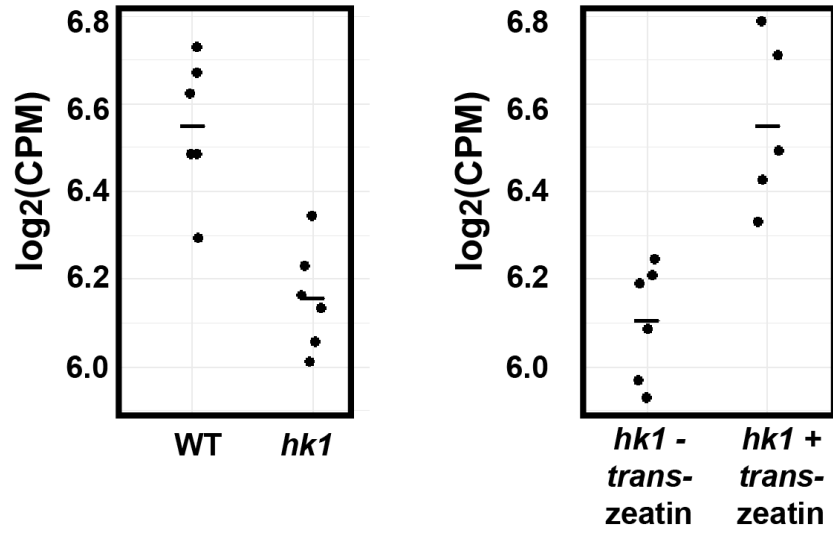
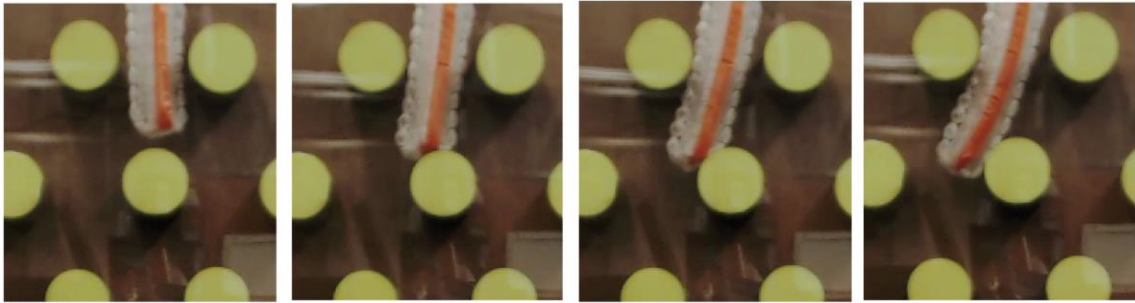


Fig. S8) $\log_2(\text{counts per million/CPM})$ for *AUX1* in wildtype vs *hk1* and *hk1* plus/minus *trans*-zeatin

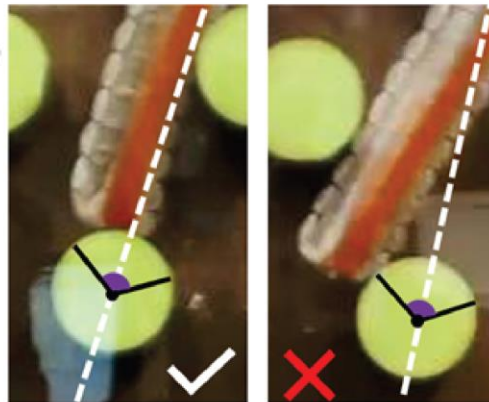
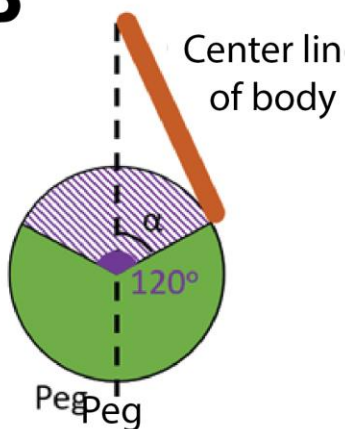
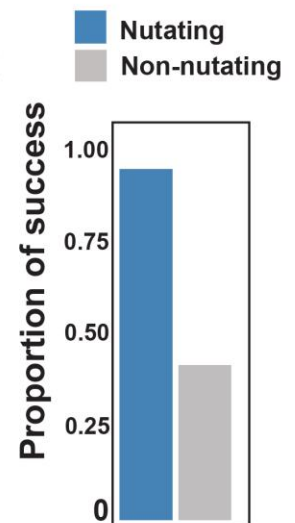
A**Nutating****Non-nutating**

0 sec

1 sec

2 sec

3 sec

B**C****Fig. S9) Definition of an “encounter” during robotic root growth**

- A) Example of nutating and non-nutating roots striking the same peg with a similar angle.
- B) The touch of the robot tip is counted as an “encounter” if the angle (α) between the line that connects the tip to the center of a peg and the line passing from the

center of a peg is less than approximately 60 degrees. The left panel shows an example of an “encounter” and the right panel does not.

- C) The overall proportion of successful obstacle clearances. 21 experiments in both conditions, with a total of $N = 59$ and 33 obstacles encountered for nutating and non-nutating, respectively. Chi-Squared test $p\text{-value} = 7.768e-10$.

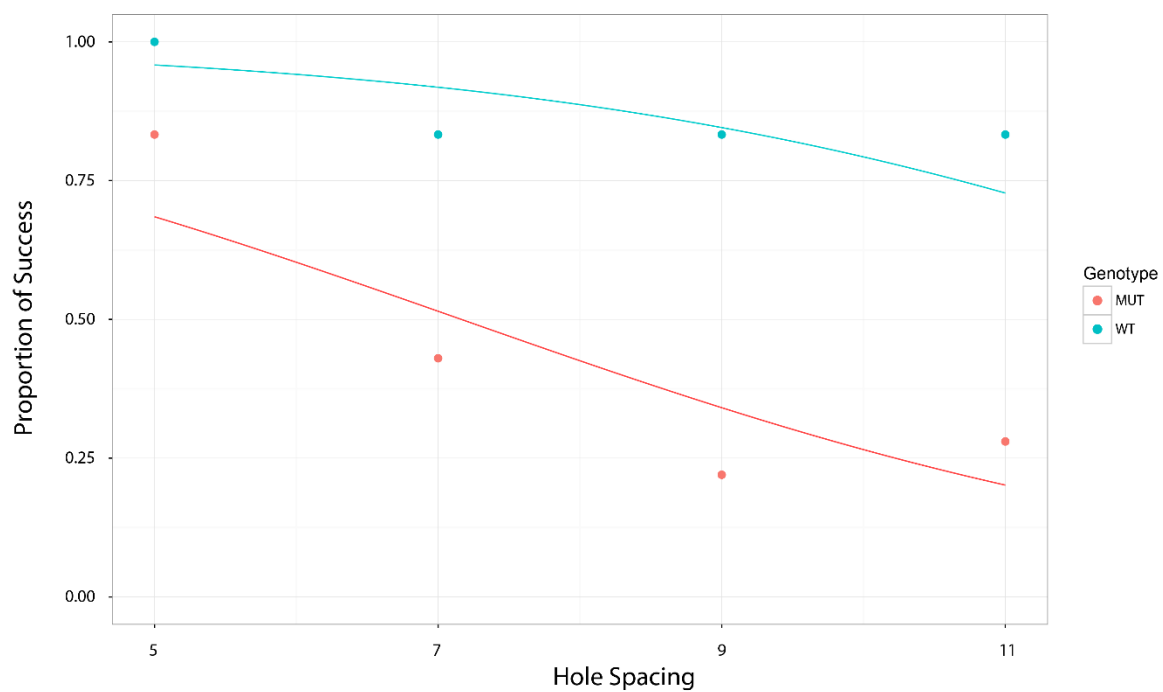


Fig. S10) Proportion of success in finding hole for wild type and mutant along with fitted logistic regression functions.

Movie S1 (separate file):

Circumnutation phenotypes of wildtype and *hkl-2*. Video depicts 105 hours of growth.

Movie S2 (separate file):

Circumnutation phenotype of wildtype before and after treatment with 1-MCP. Video depicts 86 hours of growth. 1-MCP applied at 13 second mark.

Movie S3 (separate file):

Circumnutation phenotypes of untreated *hkl-2* and *hkl-2* treated with 150 nM *trans*-zeatin. Video depicts 90 hours of growth.

Movie S4 (separate file):

Circumnutation phenotypes of untreated wildtype and wildtype treated with 40 nM NPA. Video depicts 64 hours of growth.

Movie S5 (separate file):

Circumnutation phenotypes of hydroponically grown *hkl-1* treated with 200 nM IAA, 200 nM 2-NAA, and 200 nM 1-NAA. Video depicts 41 hours of growth. Treatments were applied at the 4 second mark.

Movie S6 (separate file):

Circumnutation phenotypes of wildtype (Dongjin cultivar) and the *aux1-3* mutant. Video represents 94 hours of growth.

Movie S7 (separate file):

Surface growth phenotypes of wildtype and *hkl-1*. Video depicts 63 hours of growth.

Movie S8 (separate file):

Example circumnulating and non-circumnulating robotic simulation of root growth through an obstacle course of irregularly spaced pegs.

Movie S9 (separate file):

Germination phenotype of wildtype and *hkl-2* on clay gravel. Video depicts 109 hours of growth.

Movie S10 (separate file):

Germination phenotype of wildtype and *hkl-2* on 1.5 cm layer of clay gravel overlaying a layer of clear gel. Video depicts 135 hours of growth.

Link to supplementary datasets:

The datasets and code to reproduce statistical analyses are deposited at the Duke Research Data Repository: <https://doi.org/10.7924/r4b27x11m>

Captions for supplementary datasets:**Data S1 (separate files):**

Compressed .Rproj file containing analysis script and raw data for primary root length measurement. Open .Rproj file and run “main” script in “scripts” folder.

Data S2 (separate files):

Compressed .Rproj file containing script and raw data for root tip trace plotting. Open .Rproj file and run “main” script in “scripts” folder.

Data S3 (separate files):

Compressed .Rproj file containing analysis script and raw data for circumnutation amplitude quantification. Open .Rproj file and run “main” script in “scripts” folder.

Data S4 (separate files):

Compressed .Rproj file containing analysis script and raw data for epidermal cell length measurement. Open .Rproj file and run “main” script in “scripts” folder.

Data S5 (separate files):

Processed count files for RNA-Seq experiments.

Data S6 (separate files):

Compressed .Rproj file containing analysis script and raw data surface exploration experiment. Open .Rproj file and run “main” script in “scripts” folder.

Data S7 (separate files):

Compressed .Rproj file containing analysis script and raw data robotic root experiment. Open .Rproj file and run “main” script in “scripts” folder.

Data S8 (separate files):

Compressed .Rproj file containing analysis script and raw data for gravel penetration experiment. Open .Rproj file and run “main” script in “scripts” folder.